Two planets around Kapteyn's star: a cold and a temperate super-Earth orbiting the nearest halo red-dwarf

G. Anglada-Escudé ^{1,2*}, P. Arriagada³, M. Tuomi^{4,5}, M. Zechmeister²,

- J. S. Jenkins⁴, A. Ofir², S. Dreizler², E. Gerlach⁶, C. J. Marvin², A. Reiners²,
- S. V. Jeffers², R. Paul Butler³, S. S. Vogt⁷, P. J. Amado⁸, C. Rodríguez-López⁸,
- Z. M. Berdiñas⁸, J. Morin^{9,2}, J. D. Crane¹⁰, S. A. Shectman¹⁰, I. B. Thompson¹⁰,
- M. Díaz⁵, E. Rivera⁷, L. F. Sarmiento², H. R. A. Jones⁵
- School of Physics and Astronomy, Queen Mary, University of London, 327 Mile End Rd. London, United Kingdom
- ² Universität Göttingen, Institut für Astrophysik, Friedrich-Hund-Platz 1, 37077 Göttingen, Germany
- Carnegie Institution of Washington, Dept. of Terrestrial Magnetism, 5241 Broad Branch Rd. NW, 20015, Washington D.C., USA
- Departamento de Astronomía, Universidad de Chile, Camino El Observatorio 1515, Las Condes, Santiago, Chile, Casilla 36-D.
- ⁵ Centre for Astrophysics Research, University of Hertfordshire, College Lane, AL10 9AB, Hatfield, UK
- Institut für Planetare Geodäsie Technische Universität Dresden 01062, Dresden, Germany
- ⁷ UCO/Lick Observatory, University of California, Santa Cruz, CA, 95064, USA
- Instituto de Astrofísica de Andalucía-CSIC, Glorieta de la astronomí a S/N, 18008, Granada, Spain
- 9 LUPM-UMR5299, CNRS & Université Montpellier II, Place E. Bataillon, Montpellier, F-34095, France

Submitted April 25, 2014

ABSTRACT

Exoplanets of a few Earth masses can be now detected around nearby low-mass stars using Doppler spectroscopy. In this paper, we investigate the radial velocity variations of Kapteyn's star, which is both a sub-dwarf M-star and the nearest halo object to the Sun. The observations comprise archival and new HARPS, HIRES and PFS Doppler measurements. Two Doppler signals are detected at periods of 48 and 120 days using likelihood periodograms and a Bayesian analysis of the data. Using the same techniques, the activity indicies and archival ASAS-3 photometry show evidence for low-level activity periodicities of the order of several hundred days. However, there are no significant correlations with the radial velocity variations on the same timescales. The inclusion of planetary Keplerian signals in the model results in levels of correlated and excess white noise that are remarkably low compared to younger G, K and M dwarfs. We conclude that Kapteyn's star is most probably orbited by two super-Earth mass planets, one of which is orbiting in its circumstellar habitable zone, becoming the oldest potentially habitable planet known to date. The presence and long-term survival of a planetary system seems a remarkable feat given the peculiar origin and kinematic history of Kapteyn's star. The detection of super-Earth mass planets around halo stars provides important insights into planet-formation processes in the early days of the Milky Way.

Key words: techniques: radial velocities – stars: individual: Kapteyn's star, planetary systems

INTRODUCTION

Sub-ms⁻¹ velocity precision can now be achieved for Mdwarfs resulting from stabilized spectrographs (such as HARPS, Mayor et al. 2003) and specialized spectral analysis techniques (Anglada-Escudé & Butler 2012). This increased sensitivity enables the detection of planets of a few-Earth masses orbiting in the star's habitable zone. Recently, statistical population analyses of the NASA/Kepler mission (Dressing & Charbonneau 2013), and ground-based Doppler surveys (Bonfils et al. 2013; Tuomi et al. 2014) suggests that every low-mass star has at least one (or more) planet with

¹⁰ Carnegie Institution of Washington, The Observatories, 813 Santa Barbara Street, Pasadena, CA 91101-1292, USA

an orbital period less than 50 days. Very small planets in very short-period orbits have recently been discovered by the Kepler mission (e.g. KOI-1843, Ofir & Dreizler 2013). We recently started the Cool Tiny Beats survey to charaterise the Doppler variability over short time-scales and search for such small planets in short period orbits around nearby low-mass stars. The program uses the High Accuracy Radial velocity Planet Searcher spectrograph (HARPS) installed at the 3.6m ESO telescope at La Silla/Chile and its northern counterpart at the Telescopio Nationale Galileo/La Palma.

2 KAPTEYN'S STAR

At only 3.91 pc, Kapteyn's star (or GJ 191, HD 33793) is the closest halo star to the Sun (van Leeuwen 2007). It is subluminous with respect to main sequence stars of the same spectral type and was spectroscopically classified as an M1.0 sub-dwarf by Gizis (1997). A radius of $0.291\pm0.025~\mathrm{R}_{\odot}$ was directly measured by Ségransan et al. (2003) using interferometry. This combined with an estimate of its total luminosity was then used to derive an effective temperature of 3570 ± 156 K and its mass was estimated to be 0.281 ± 0.014 M_{\odot} . Woolf & Wallerstein (2005) determined a metallicity of [M/H] = -0.86 which coincides with several later estimates within 0.05 dex. We independently obtained estimates of its metallicity and temperature by comparing its observed colors (B, V, J, H, and K) to synthetically generated ones from the PHOENIX library (Husser et al. 2013), obtaining compatible values of [Fe/H] = -0.89 and 3550 ± 50 K. Only an upper limit has been measured for its projected rotation velocity $(v \sin i < 3 \text{kms}^{-1})$, Browning et al. 2010), and its X-ray luminosity has been measured to be comparable to other multi-planet host M-dwarfs such as GJ 876 and GJ 581 (Walkowicz et al. 2008). Therefore, planets of a few Earth-masses orbiting such an inactive M-star should be detectable using Doppler spectroscopy (Barnes et al. 2011). A precise age estimation of the star cannot be obtained from models, as they change very little for $M < 0.6 M_{\odot}$ in the range of ages between 0.4 and 15 Gyr (Baraffe et al. 1997; Ségransan et al. 2003). The low metallicity and halo kinematics suggest an ancient origin, which is consistent with its low-activity and slow rotation.

3 OBSERVATIONS

The observations comprise both new and archival data from HARPS, HIRES and PFS spectrometers. HARPS is a stabilized high-resolution spectrometer (resolving power ~ 110 000) covering from 380 to 680 nm. The HARPS data we use come from two programs; the Cool Tiny Beats survey and archival data from the first HARPS-GTO survey. The Cool Tiny Beats data were obtained in two 12 night runs in May 2013 (11 spectra) and in Dec 2013 (55 spectra). The HARPS-GTO data contain 30 spectra taken between 2003 and 2009. Bonfils et al. (2013) reported some possible signals on Kapteyn's star, but no detection claim could be made at the time. Doppler measurements were obtained using the least-squares template-matching approach as implemented by the HARPS-TERRA software (Anglada-Escudé & Butler 2012). For each spectrum, we

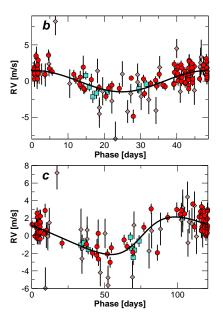


Figure 2. Phase folded Doppler curves to the reported signals with the other signal removed (HARPS are red circles, HIRES are brown diamonds and PFS are blue squares). The maximum likelihood solution is depicted as a black line.

also use two measurements of the symmetry of the meanline profile as provided by the HARPS-Data Reduction Software. These are the bisector span (BIS) and the full-widthat-half-maximum (FWHM) of the cross-correlation function. BIS and FWHM are known to correlate with activity induced features that can cause spurious Doppler signals. For example, changes in the line-symmetry caused by co-rotating dark and magnetic spots induce changes in the symmetry of the lines that produce spurious Doppler shifts (e.g., Reiners et al. 2013). The variability in the Ca II H+K emission lines was also measured by HARPS-TERRA through the S-index. The variability in the S-index is also known to correlate with magnetic activity of the star (Gomes da Silva et al. 2012), and localized active regions such as spots. Any Doppler signal with a period equivalent to variability detected in the BIS, FWHM and S-index is likely to be spurious.

We include 30 Doppler measurements spanning between 1999 and 2008 using the HIRES spectrometer at Keck (Vogt et al. 1994). These measurements were obtained using the Iodine cell technique as described in Butler et al. (1996). A new HIRES stellar template was generated by deconvolving a high signal-to-noise iodine-free spectrum of the star applying Maximum Likelihood deconvolution with Boosting (Morháč & Matouøsec 2009). The star is never at an altitude greater than 26 deg from Hawaii, which could explain the lower accuracy compared to the HARPS measurements. The long baseline of HIRES puts strong constraints on the long-period variability and mitigates alias ambiguities in the HARPS data. We also included 8 new Doppler measurements obtained with PFS Crane et al. (2010) at Magellan/Las Campanas observatory, also using the Iodine cell technique. While the statistical contribution of PFS is small, the significance of the preferred solution increases thus providing further support to the signals. All spectroscopic measurements used are given in table 1.

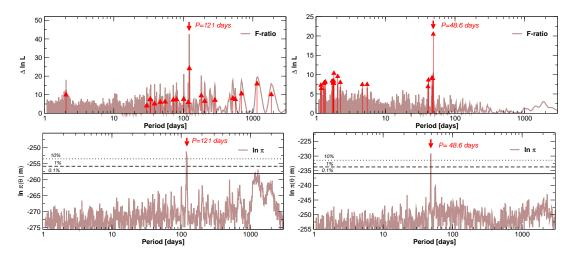


Figure 1. Top panels illustrate the detection periodograms for a model with one-planet (left), and the search for the second signal (right). Brown thick line is the F-ratio periodogram applied to residual data, it does not adjust for the extra-white noise as a free parameter and is only used to initialize the global maximum-likelihood searches. Red triangles represent the top twenty likelihood maxima. Bottom panels show the Posterior probability contours as obtained by tempered MCMC samplings using the DRAM algorithm (see text). Horizontal lines indicate relative probability thresholds compared to the maximum posterior. For perfectly known uncertainties and in the absence of correlations, the F-ratio and the log-likelihood ratio statistic should coincide. However, this is hardly the case when dealing with Doppler data. Top panels also illustrate the perils of working with residual data statistics to assess significance of signals. That is, the F-ratio is over-optimistic in the significance of the first candidate (left panel, 121 days brown peak is much higher), while the significance of the second signal at 48.6 days (right panel) would be greatly underestimated.

Table 1. Spectroscopic measurements. Median value and a perspective acceleration were subtracted to each RVs set (Ins. 1 is HARPS, 2 is HIRES, 3 is PFS). FWHM, BIS, and S-index are provided for HARPS only. Uncertainty in the FWHM is $2.5 \times \sigma_{BIS}$.

i	RV [ms ⁻¹]	$[\text{ms}^{-1}]$	Ins	$_{[ms}^{BIS}$	${\sigma_{\rm BIS} \atop [{ m ms}^{-1}]}$	FWHM [kms ⁻¹]	S-index [-]	$\sigma_{\text{S-index}}$
2452985.74111 3	3.11	0.80	1	-4.64	0.86	3.21561	0.2966	0.0042
2452996.76321 3	3.00	0.27	1	-9.75	0.56	3.19206	0.2699	0.0033
2453337.80096 -	2.65	0.89	1	-8.17	0.76	3.18036	0.1859	0.0036
2453668.83537 -	2.57	0.52	1	-10.27	0.49	3.21216	0.2678	0.0026

4 SIGNAL DETECTION METHODS

The initial signal detection is performed using log-likelihood periodograms (Baluev 2009; Anglada-Escudé et al. 2013) and tempered Markov Chain samplings using the delayed-rejection adaptive-Metropolis method (or DRAM, Haario et al. 2006) as implemented in Tuomi et al. (2014). These methods produce maps of the maximum likelihood and posterior densities as a function of the period being investigated. As in classic periodograms, preferred periods will appear as peaks (local probability maxima). The significance is then assessed using the Bayesian criteria described in Tuomi et al. (2014). We say that a Doppler signal is detected if 1) its period is well-constrained, 2) its amplitude is statistically significantly different from zero, and 3) inclusion of the signal in the model increases the Bayesian evidence by a factor of 10⁴, which is more conservative than usual because important effects might be missing in the model, especially when combining data from different instruments. The model of the observations is fully encoded in the definition of the likelihood function. In addition to the usual Keplerian parameters, our model includes three nuisance parameters for each instrument (INS): a constant offset γ_{INS} , an extra white-noise term σ_{INS}

and a Moving Average coefficient ϕ_{INS} that quantifies the amount of correlation between consecutive measurements. ϕ_{INS} is bound between +1 and -1 (anticorrelation) and a value consistent with zero implies no significant correlation. Our model also assumes an exponential decay of the correlation that depends on a characteristic time-scale τ_{INS} . Adding it as a free parameter led to overparameterization, so a fixed value of $\tau_{\text{INS}} = 4$ days was set by default. Linear trends caused by the presence of planets with periods much longer than the time-baseline is parameterized as $\dot{\gamma}(t_i - t_0)$, where $\dot{\gamma}$ is also a free parameter of the Doppler model and t_0 is an arbitrary reference epoch (see Table 2). The log-likelihood periodograms use the same likelihood model but do not include correlations terms. False alarm probability assessments using likelihood periodograms (or FAP, see Baluev 2008) are also computed to double-check the significance of each detection.

5 ANALYSIS OF THE TIME-SERIES

The search for signals in the Doppler time-series is summarized in Figure 1. Two very significant periods are detected at 121 and 48.6 days. The Bayesian evidence ratios

Table 2. The Keplerian solution of the combined radial velocities presented as median of the posterior estimates and corresponding 68% credibility intervals. The uncertainties of semi-major axes and minimum masses include uncertainties in the stellar mass. Reference epoch t_0 for computation of M_0 (mean anomaly) and λ_0 (mean longitude) is assumed to be JD=2452985.74111 days.

Model parameter	Kapteyn b	Kapteyn c
$P [\text{day}]$ $K [\text{ms}^{-1}]$ e $\omega [\text{deg}]$ $M_0 [\text{deg}]$ $\dot{\gamma} [\text{ms}^{-1} \text{yr}^{-1}]$ $\sigma_{\text{HARPS}} [\text{ms}^{-1}]$ $\sigma_{\text{PFS}} [\text{ms}^{-1}]$ ϕ_{HARPS} ϕ_{HIRES} ϕ_{PFS}	$\begin{array}{c} 48.616^{+0.036}_{-0.032} \\ 2.25^{+0.31}_{-0.10} \\ 2.25^{+0.31}_{-0.10} \\ 80.4^{+30.7}_{-2.00} \\ 269.6^{+38.3}_{-32.2} \\ -0.181^{+0.086}_{-0.086} \\ 0.65^{+0.10}_{-0.10} \\ 1.17^{+0.51}_{-0.47} \\ 0.32^{+0.69}_{-0.08} \\ 0.40^{+0.50}_{-0.30} \\ 0.10^{+0.30}_{-0.30} \end{array}$	$121.54_{-0.25}^{+0.25} \\ 2.27_{-0.26}^{+0.28} \\ 2.27_{-0.26}^{+0.10} \\ 0.23_{-0.12}^{+0.10} \\ 3.9_{-33.2}^{+28.9} \\ 357.6_{-27.9}^{+32.3}$
Derived quantities		
$\lambda_0 = \omega + M_0 \text{ [deg]}$ $m_p \sin i \text{ [M}_{\oplus}\text{]}$ $a \text{ [AU]}$ S/S_{\oplus} $HZ\text{-range [AU]}$ P_c/P_b	$\begin{array}{c} 350^{+19.1}_{-18.7} \\ 4.8^{+0.9}_{-1.0} \\ 0.168^{+0.006}_{-0.008} \\ 40\% \\ \sim & 0.126^{+0.021}_{-0.029} \end{array}$	$1.6^{+20.5}_{-20.1}$ $7.0^{+1.2}_{-1.0}$ $0.311^{0.038}_{0.014}$ 12%

are 3.2×10^9 for the one-planet model against the no-planet model, and 3.1×10^9 for the two-planet solution against the one-planet model. These numbers are well in excess of the 10⁴ threshold indicating very confident detections. The FAPs as derived from the log-likelihood periodograms are 1.5×10^{-6} and 8.9×10^{-5} respectively, which are also very small further supporting the detections (acceptable detection thresholds using periodogram methods are typically between 1% and 0.1%). The support of the signals by the three data sets is illustrated in the phase-folded curves in Figure 2. The uneven sampling can produce biases in the significance estimates. To investigate this, we also performed the same analysis using nightly averaged measurements. The same two signals are detected well above our significance thresholds, thus providing further confidence in the detections. As for other stars, further follow-up over the next few years is desirable to confirm that both low-amplitude signals remain coherent over time.

We investigated linear correlations with activity indices by including them in the likelihood model of the HARPS data. While we could still easily detect the planetary signals, these models had lower probabilities due to overparameterization and are not included in the final solution. We also verified whether if any indicator of activity showed variability in similar time-scales as the Doppler data. While the BIS does not show any hint of temporal coherence, the FWHM and S-index do share similar periodogram structures with tentative peaks between 140 to 2000 days. However, neither had FAPs that were lower than 5%, indicating little significance.

We also analysed V-band photometry obtained from the latest release of the ASAS program (Pojmanski 1997)¹. A standard deviation computed using the central 80% percentile was used to remove $4-\sigma$ outliers resulting in 503 epochs spanning from Dec 2000 to Sep 2007. A log-likelihood periodogram analysis identified two significant signals at 340 and 1100 days, both with amplitudes of ~ 5 mmag. The signal at 1100 days is compatible with other reports of periodicities in activity indices of M-dwarfs (Gomes da Silva et al. 2012), and the 340-day variability might be caused by seasonal systematic errors, or by a long rotation period. The periodogram structure of the photometry resembles those of the FWHM and the S-index, further supporting potential low-level activity changes happening at timescales of several hundred days. Given that the activity and Doppler signals appear uncorrelated, we conclude that the simplest interpretation of the Doppler data is the presence of two planets (see Table 2). With a period of 48.6 days, Kapteyn b lies well within the liquid water habitable zone of the star (Kopparapu et al. 2013). Assuming rocky composition, its properties and possible climates should be similar to those discussed for GJ 667Ce (Anglada-Escudé et al. 2013). Kapteyn c receives $\sim 10\%$ of Earth's irradiance, implying that the possibility of it being able to support liquid water on its surface is less probable.

We used Optimal BLS (Ofir 2014) to search for possible transit events in the ASAS photometry. No trasits were found when searching for a signal in the range of parameters compatible with the Doppler solution. Further observations at the predicted transit windows are needed to put meaningful constraints on possible transit signals.

6 DISCUSSION

The age of Kapteyn star can be inferred from its membership to the Galactic halo and peculiar element abundances (Kotoneva et al. 2005). The current hierarchical Milky Way formation scenario suggests that streams of halo stars were originated as tidal debris from satellite dwarf galaxies being engulfed by the early Milky Way (Klement 2010, and references therein). This scenario is supported by the age estimations of the stars in the inner halo ($\sim 10-12$ Gyr, Jofré & Weiss 2011), and globular clusters. The work by Eggen and collaborators (see, Eggen 1996, as review summary) established the existence of such high-velocity, metalpoor moving groups in the solar neighborhood. Kapteyn's star is the prototype member of one of these groups, which has been recently investigated by Wylie-de Boer et al. (2010) among others. Stars in Kapteyn's group share a retrograde velocity of rotation around the Galactic centre of about -290 kms⁻¹ (Eggen 1996). Spectroscopic observation of 16 members has shown that the group likely originated from the same progenitor structure as the peculiar globular cluster ω Centauri, but not from within the cluster itself (Kotoneva et al. 2005; Wylie-de Boer et al. 2010). The origin of Kapteyn's star within a merging dwarf-galaxy sets its most likely age around the young halo's one (> 10 Gyr) and should not be older than 13.7 Gyrs, which is the current

¹ ASAS-3 release http://www.astrouw.edu.pl/asas/?page=catalogues

estimate of the age of the universe (Planck Collaboration 2013).

Numerical integration of several possible orbits over 10^4 yr to 1 Myr using Mercury 6 (Chambers 1999) shows very small changes in the orbital parameters. Despite the the periods for the two planet candidates are compatible with a 5:2 period commensurability (see Table 2), the analysis of the resonant angles for the best fit solution did not support the presence of dynamical mean-motion resonances, which existence also depend on a number of other properties such total planet masses and mutual inclinations. We found, however, that the difference in periastron angles $\Delta\omega = \omega_b - \omega_c$ librates around 180 deg; which corresponds to a long-term stable configuration called apsidal locking. This is sufficient to show that the proposed system is compatible with long-term physically-viable solutions. It has been suggested that two-planet systems that underwent weak dissipation (slow migration) should always end-up in absidal locking (Michtchenko & Rodríguez 2011), which has consequences on the likely planet-formation scenario. A more thorough analysis to properly quantify the significance of the absidal locking and possible mean-motion ressonances requires a much more extended discussion (e.g., Anglada-Escudé et al. 2013) which is beyond the scope of this paper.

The detection of two super-Earths here is consistent with the idea that low-metallicity stars are more prone to the formation of low-mass planets rather than gas giants (Udry & Santos 2007; Buchhave et al. 2012). This is further supported by a significant paucity of lowest-mass planets in Doppler searches of metal-rich stars Jenkins et al. (2013), and non-comfirmation of previous claims of gas giants around extremely metal-poor stars (Desidera et al. 2013; Jones & Jenkins 2014). These observational findings are compatible with recent population synthesis experiments such as those in Mordasini et al. (2012).

Once the planets signals are included in the Doppler model, the RV residuals variability are reduced to instrumental noise (i.e. extra jitter term is compatible with reported stability of HARPS, and correlation coefficients compatible with 0). This indicates that the star is very Doppler stable, possibly more stable than the instruments themselves. This indeed would be expected because pulsation and convective motions are thought to be much smaller in inactive low-mass stars than in earlier types. At the likely age of the system, most G and K dwarfs are evolving away from the main sequence into giants, which makes the Doppler detection of small planets unfeasible due to increased activity levels (e.g., Nowak et al. 2013). As a result, original architectures of the first planetary systems can only be explored by observing venerable low-mass stars which are still on the main-sequence such as Kapteyn's star.

Acknowledgments. We thank R.P.Nelson, J.Chanamé and R. Baluev (referee) for constructive comments and discussions. We acknowledge funding from: DFG/Germany through CRC-963 (CJM); DFG/Germany 1664/9-1 (AR); Alexander Von Humboldt Foundation/Germany (JM); ERC-FP7/EU grant number 27347 (MZ), AYA2011-30147-C03-01 by MINECO/Spain, FEDER funds/EU, and 2011 FQM 7363 of Junta de Andalucía/Spain (CR-L and PJA); JAE-Doc program (CR-L); FPI BES-2011-049647 MINECO/Spain (ZMB); CATA (PB06, CONICYT)/Chile (JSJ); CONICYT-PFCHA/Doctorado Na-

cional/Chile (MD);NSF/USA grants AST-0307493 and AST-0908870 (SSV); and NASA grant NNX13AF60G S02 (RPB). Based on observations made with ESO Telescopes under programme ID 191.C-0505 and ESO's Science Archive Facility (req. number GANGLADA95087). We acknowledges the effort of the HARPS team program obtaining data within program 072.C-0488. Some data were obtained at the W.M. Keck Obs. made possible by the support of the W.M. Keck Foundation and operated among Caltech, Univ. of California and NASA. The authors are most fortunate to conduct observations from the sacred mountain of Mauna Kea. This study uses data obtained at Magellan, operated by the Carnegie Inst., Harvard Univ., Univ. of Michigan, Univ. of Arizona, and the Massachusetts Inst. of Technology.

REFERENCES

Anglada-Escudé G., Butler R. P., 2012, ApJS, 200, 15 Anglada-Escudé G., Tuomi M., Gerlach E., et al. 2013, A&A, 556, A126

Baluev R. V., 2008, MNRAS, 385, 1279

Baluev R. V., 2009, MNRAS, 393, 969

Baraffe I., Chabrier G., Allard F., Hauschildt P. H., 1997, A&A, 327, 1054

Barnes J. R., Jeffers S. V., Jones H. R. A., 2011, MNRAS, 412, 1599

Bonfils X., Delfosse X., Udry S., et al. 2013, A&A, 549, A109

Browning M. K., Basri G., Marcy G. W., West A. A., Zhang J., 2010, AJ, 139, 504

Buchhave L. A., Latham D. W., Johansen A., et al. 2012, Nature, 486, 375

Butler R. P., Marcy G. W., Williams E., et al. 1996, PASP, 108, 500

Chambers J. E., 1999, MNRAS, 304, 793

Crane J. D., Shectman S. A., Butler R. P., et al. 2010, Proc. SPIE, 7735

Desidera S., Sozzetti A., Bonomo A. S., et al. 2013, A&A, 554, A29

Dressing C. D., Charbonneau D., 2013, ApJ, 767, 95

Eggen O. J., 1996, AJ, 112, 1595

Gizis J. E., 1997, AJ, 113, 806

Gomes da Silva J., Santos N. C., Bonfils X., et al. 2012, A&A, 541, A9

Haario H., Laine M., Mira A., Saksman E., 2006, Statistics and Computing, 16, 339

Husser T.-O., Wende-von Berg S., Dreizler S., et al. 2013, A&A, 553, A6

Jenkins J. S., Jones H. R. A., Tuomi M., et al. 2013, ApJ, 766, 67

Jofré P., Weiss A., 2011, A&A, 533, A59

Jones M. I., Jenkins J. S., 2014, A&A, 562, A129

Klement R. J., 2010, A&A Rev., 18, 567

Kopparapu R. K., Ramirez R., Kasting et al. 2013, ApJ, 765, 131

Kotoneva E., Innanen K., Dawson P. C., et al. 2005, A&A, 438, 957

Mayor M., Pepe F., Queloz D., Bouchy F., et al. 2003, The Messenger, 114, 20

Michtchenko T. A., Rodríguez A., 2011, MNRAS, 415, 2275

Mordasini C., Alibert Y., Benz W., Klahr H., Henning T., 2012, A&A, 541, A97

Morháč M., Matouøsec V., 2009, DSP, 19, 372

Nowak G., Niedzielski A., Wolszczan A., Adamów M., Maciejewski G., 2013, ApJ, 770, 53

Ofir A., 2014, A&A, 561, A138

Ofir A., Dreizler S., 2013, A&A, 555, A58

Planck Collaboration 2013, arXiv:1303.5062

Pojmanski G., 1997, AcA, 47, 467

Reiners A., Shulyak D., Anglada-Escudé G., et al. 2013, A&A, 552, A103

Ségransan D., Kervella P., Forveille T., Queloz D., 2003, A&A, 397, L5

Tuomi M., Anglada-Escude G., Jenkins J. S., Jones H. R. A., 2014, arXiv:1405.2016

Tuomi M., Jones H. R. A., Barnes J. R., et al. 2014, MN-RAS

Udry S., Santos N. C., 2007, ARA&A, 45, 397

van Leeuwen F., 2007, A&A, 474, 653

Vogt S. S., Allen S. L., Bigelow B. C., et al. 1994, SPIE Conf. Series, 2198, 362

Walkowicz L. M., Johns-Krull C. M., Hawley S. L., 2008, ApJ, 677, 593

Woolf V. M., Wallerstein G., 2005, MNRAS, 356, 963

Wylie-de Boer E., Freeman K., Williams M., 2010, AJ, 139, 636

APPENDIX A: ON-LINE TABLE

Spectroscopic measurements on Kapteyn's star (Anglada-Escude+, 2014)

Description:

Time-series of spectroscopic measurements used in the paper. Median value and a perspective acceleration were subtracted to each RVs set (Ins. 1 is HARPS, 2 is HIRES, 3 is PFS). Measurements of the FWHM, BIS of the cross-correlation profiles and measurements of the S-index are provided for HARPS data only. Uncertainty in the FWHM is 2.5 times the uncertainty in BIS. Check 2012ApJS..200...15A, for more detailed definitions of the measurements and their uses.

Bytes	Format	Units	Label	Explanations
1- 13 15- 19 21- 24 26 28- 33 35- 38 40- 46 48- 53	F4.2 I1 F6.2 F4.2 F7.5	m/s m/s m/s m/s km/s	JD RVel eRVel Ins BIS eBIS FWHM Sidx	Barycentric Julian date Radial velocity Uncertainy in RV Instrument used Bisector span of the CCF Uncertainty in BIS FWHM of the CCF (1) CaII H+K S-index in the Mount Wilson system
55- 60	F6.4		eSidx	Uncertainty in S-index

Note (1): Uncertainty in FWHM is 2.5x eBIS

```
2452985.74111 3.11 0.80 1 -4.64 0.86 3.21561 0.2966 0.0042
2452996.76321 3.00 0.27 1 -9.75 0.56 3.19206 0.2699 0.0033
2453337.80096 -2.65 0.89 1 -8.17 0.76 3.18036 0.1859 0.0036
2453668.83537 -2.57 0.52 1 -10.27 0.49 3.21216 0.2678 0.0026
2453670.73947 -3.76 0.59 1 -13.27 0.41 3.20937 0.2636 0.0022
2454167.53053 -1.22 0.56 1 -14.86 0.38 3.20717 0.2616 0.0020
2454169.50521 -1.66 0.48 1 -13.34 0.34 3.19959 0.2578 0.0018
2454173.50080 -1.57 0.48 1 -13.76 0.36 3.19892 0.2540 0.0019
2454345.87966 0.29 0.45 1 -12.34 0.33 3.20096 0.2549 0.0017
2454424.73161 2.40 0.54 1 -14.00 0.37 3.19613 0.2305 0.0018
2454449.76051 1.27 0.61 1 -13.88 0.45 3.18970 0.2318 0.0023
2454450.64700 1.67 0.57 1 -13.85 0.40 3.19968 0.2346 0.0020
2454733.89725 -0.93 0.60 1 -15.14 0.36 3.20390 0.2536 0.0018
2454754.83883 -2.37 0.57 1 -13.84 0.41 3.20737 0.2538 0.0021
2454879.55605 -2.33 0.59 1 -15.14 0.43 3.19513 0.4865 0.0032
2454879.69685 -1.36 0.85 1 -14.42 0.68 3.19309 0.2085 0.0034
2454880.52165 -0.01 1.56 1 -0.65 1.28 3.19636 0.2472 0.0053
2454880.67387 -2.96 0.76 1 -13.39 0.57 3.19398 0.2071 0.0028
```

```
2456417.46007 -0.10 0.60 1 -14.56 0.68 3.20851 0.2682 0.0044
2456417.46745 -0.54 0.68 1 -7.42 0.75 3.20894 0.2566 0.0047
2456418.46471 1.80 0.43 1 -16.75 0.55 3.20068 0.2761 0.0040
2456420.47541 0.63 0.39 1 -15.72 0.47 3.19810 0.3089 0.0037
2456421.46438 1.82 0.76 1 -18.81 0.95 3.20174 0.2652 0.0056
2456422.45767 2.00 0.72 1 -13.54 0.71 3.19709 0.2700 0.0049
2456424.44602 1.03 0.93 1 -7.98 0.95 3.20863 0.4363 0.0069
2456427.44860 3.42 0.75 1 -14.61 0.78 3.20405 0.2690 0.0050
2456428.46156 1.08 0.55 1 -10.70 0.68 3.20416 0.4196 0.0058
2456656.69364 3.00 0.55 1 -12.33 0.55 3.20616 0.2597 0.0037
2456656.74624 1.87 0.58 1 -15.74 0.55 3.20590 0.2707 0.0037
2456657.55783 1.33 0.75 1 -16.59 0.62 3.21076 0.2827 0.0040
2456657.59109 2.32 0.53 1 -13.13 0.58 3.20375 0.2525 0.0037
2456657.70141 2.59 0.57 1 -19.43 0.52 3.19999 0.2884 0.0040
2456657.75751  0.63  0.62  1 -19.62  0.50  3.21424  0.2675  0.0032
2456658.60490 1.03 0.51 1 -13.50 0.57 3.21336 0.2671 0.0036
2456658.70151
       1.26 0.65 1 -18.40 0.51 3.22847 0.2596 0.0029
2456659.63210 1.86 0.53 1 -17.67 0.47 3.21368 0.2745 0.0030
2456659.79823 1.45 0.66 1 -10.39 0.54 3.19687 0.2690 0.0040
2456660.68361 2.24 0.61 1 -15.18 0.55 3.20553 0.2735 0.0038
2456660.74382 1.46 0.63 1 -15.76 0.66 3.21245 0.2705 0.0042
2456660.79408 3.28 0.76 1 -16.45 0.83 3.20489 0.2632 0.0051
2456660.82165 3.14 0.98 1 -10.63 1.01 3.20620 0.3202 0.0065
2456661.56643 2.21 0.55 1 -12.63 0.56 3.20931 0.2886 0.0037
2456661.65691 0.66 0.52 1 -11.49 0.57 3.21339 0.2699 0.0038
2456665.54012 3.21 0.62 1 -15.37 0.55 3.21136 0.2941 0.0035
2456665.66524 2.73 0.69 1 -15.27 0.66 3.21198 0.2955 0.0046
2456665.68169
       0.33 0.65 1 -17.38 0.60 3.21303 0.2737 0.0040
2456665.69927 1.95 0.59 1 -15.54 0.61 3.21404 0.2957 0.0043
2456665.73292 1.00 0.71 1 -12.16 0.64 3.20612 0.2586 0.0042
2456666.62771 1.60 0.59 1 -18.01 0.59 3.22144 0.2866 0.0039
2456666.67780 0.95 0.64 1 -14.63 0.63 3.21306 0.2783 0.0043
2456666.74492 1.06 0.62 1 -15.17 0.59 3.20733 0.2932 0.0045
```

```
2456667.67412 2.21 0.79 1 -16.97 0.72 3.21627 0.3009 0.0049
2456667.74602 1.04 0.57 1 -14.67 0.64 3.20707 0.3147 0.0048
2456667.79693 2.86 0.72 1 -9.98 0.78 3.21002 0.2869 0.0052
2451170.92507 5.00 1.59 2 0.00 0.00 0.00000 0.0000 0.0000
2451580.81122 -4.06 1.71 2 0.00 0.00 0.00000 0.0000 0.0000
2452189.14851 1.79 2.37 2 0.00 0.00 0.00000 0.0000 0.0000
2452235.90051 -0.81 1.98 2 0.00 0.00 0.00000 0.0000 0.0000
2452538.06980 7.73 1.88 2 0.00 0.00 0.00000 0.0000 0.0000
2452651.88827 -7.96 2.36 2 0.00 0.00 0.00000 0.0000 0.0000
2452711.72343 -5.73 1.85 2
                       0.00 0.00 0.00000 0.0000 0.0000
2453339.97662 -1.19 1.85 2 0.00 0.00 0.00000 0.0000 0.0000
2453368.91795  0.24  1.96  2  0.00  0.00  0.00000  0.0000  0.0000
2453425.72302 -6.66 1.38 2 0.00 0.00 0.00000 0.0000 0.0000
2453425.72927 -7.53 1.88 2 0.00 0.00 0.00000 0.0000 0.0000
2453723.91920 1.93 1.74 2 0.00 0.00 0.00000 0.0000 0.0000
2453776.76985 -1.62 1.52 2 0.00 0.00 0.00000 0.0000 0.0000
2453776.77608 -2.64 1.50 2 0.00 0.00 0.00000 0.0000 0.0000
2453982.10746 4.57 1.30 2 0.00 0.00 0.00000 0.0000 0.0000
2454085.98215 3.44 2.05 2 0.00 0.00 0.00000 0.0000 0.0000
2454138.73882 -1.22 1.57 2
                        0.00 0.00 0.00000 0.0000 0.0000
2454398.04694 -1.97 1.66 2 0.00 0.00 0.00000 0.0000 0.0000
2454430.03169 0.71 1.99 2 0.00 0.00 0.00000 0.0000 0.0000
2454454.98751 -3.58 1.56 2 0.00 0.00 0.00000 0.0000 0.0000
2454455.85705 -1.14 1.31 2 0.00 0.00 0.00000 0.0000 0.0000
2454460.82264 -2.21 1.97 2 0.00 0.00 0.00000 0.0000 0.0000
2454718.13512 1.39 1.52 2 0.00 0.00 0.00000 0.0000 0.0000
2454723.12422 0.03 1.45 2 0.00 0.00 0.00000 0.0000 0.0000
2454724.13185 -0.17 1.57 2 0.00 0.00 0.00000 0.0000 0.0000
2454725.14330 1.29 1.68 2 0.00 0.00 0.00000 0.0000 0.0000
2455490.97157 -5.19 1.53 2 0.00 0.00 0.00000 0.0000 0.0000
2456695.57403 -0.31 0.64 3 0.00 0.00 0.00000 0.0000 0.0000
2456697.60659 0.21 0.54 3
                        0.00 0.00 0.00000 0.0000 0.0000
2456700.62164 0.00 0.53 3
                        0.00 0.00 0.00000 0.0000 0.0000
2456730.55791 -0.06 0.57 3 0.00 0.00 0.00000 0.0000 0.0000
2456731.52289 -1.26 0.84 3 0.00 0.00 0.00000 0.0000 0.0000
2456732.54351 -0.59 0.77 3 0.00 0.00 0.00000 0.0000 0.0000
2456735.53824  0.06  0.65  3  0.00  0.00  0.00000  0.0000  0.0000
```